Analogs in the Wintertime 500 mb Height Field

DAVID S. GUTZLER[1] AND JAGADISH SHUKLA

Goddard Laboratory for Atmospheric Sciences, NASA/Goddard Space Flight Center, Greenbelt, MD 20771

(Manuscript received 9 March 1983, in final form 16 September 1983)

ABSTRACT

A 15-winter sample of daily gridded values of Northern Hemisphere 500 mb heights is examined for the existence of recurrent flow patterns ("analogs"). The analog search is repeated several times after degrees of freedom are successively removed from the data by spatial filtering, temporal averaging, and consideration of smaller sectors of the hemisphere. The root mean square difference (or "rms error") between the most closely analogous maps, defined over the middle latitudes (30–70°N), is slightly greater than half the average error between randomly chosen maps, with an estimated rms error doubling time of nearly 8 days. If the analog search is conducted using only the long-wave component (zonal wavenumbers 0–4) of each map, the rms error between the best analog pairs is reduced to less than half of the rms error between long-wave anomalies on randomly chosen maps, but the doubling time is also reduced to less than 7 days. If the analog search is further restricted to a limited region over North America or Europe, the rms error between the best analog pairs is less than 40% of the rms error (for the sme region) between randomly chosen maps, but the error doubling time is further reduced to 4–5 days. In all cases, the degradation of analog quality is so rapid that a forecasting scheme based on the analogs would fail to produce more skillful forecasts than simple persistence.

1. Introduction

The possibility that an atmospheric circulation pattern might recur at some time in the distant future, defining a pair of analogous flows or "analogs", was considered by Lorenz (1969b). Lorenz desired to calculate the rate at which small differences between synoptic circulation patterns grew into large differences, thereby providing an empirical estimate of atmospheric predictability. He was hindered from making a definitive statement concerning the growth rate of small errors by the discovery that his data set did not include even a single pair of "good" analogs— that is, no two circulation patterns were so similar that each could be considered representative of the same flow, differing only by a small "error" of the same magnitude as a measurement error.

However, the concept of analogous circulation patterns has been used to make marginally skillful forecasts by climatologists considering time-averaged fields. Baur (1948) catalogued recurrent circulation patterns over the North Atlantic Ocean and Europe into Grosswetterlagen. The Grosswetterlagen have been used by Schuurmans (1973) to make 30-day temperature forecasts. On a global scale, circulation analogs in the form of teleconnection patterns occurring in seasonal mean pressure and temperature fields were documented many years ago by Walker and Bliss (1932). On shorter time scales, 5-day mean teleconnection patterns in the 700 mb height field (Martin, 1953; O'Connor, 1969) have been used by the U.S. Weather Service as an aid to extended range forecasting. More recently, Barnett and Preisendorfer (1978) defined a "climate state vector" which they used to forecast seasonal average surface air temperatures over North America.

It is possible that Lorenz did not find good analogs because the instantaneous, three-dimensional circulation patterns he examined contained many more degrees of freedom than the simpler time-averaged fields considered by the others. Lorenz calculated the rms differences between gridded maps of geopotential height at three levels over the Northern Hemisphere. The Grosswetterlagen, by contrast, were based on a much more limited area, and were defined using data at a single level. In addition, much of the small scale structure in the synoptic data is filtered out in the time-averaging process. The teleconnection patterns are even simpler: they are based on correlations between individual grid points without regard to the complete hemispheric circulation pattern. The regional character of the patterns was demonstrated by Horel (1981), who reproduced the teleconnection patterns documented by Wallace and Gutzler (1981) using a hemispheric empirical orthogonal function scheme which incorporated cluster analysis to maximize local instead of global variance.

[1] Current affiliation: Department of Earth, Atmospheric, and Planetary Sciences, Massachusetts Institute of Technology, Cambridge, MA 02139.

Apparently, the complete hemispheric three-dimensional structure of tropospheric flow contains too many degrees of freedom to hope for good analogs. Considering the strong evidence for analog-type structures in time-averaged fields, we were motivated by the following questions:

- Could we find better analog pairs of instantaneous flow patterns if we considered only the middle latitudes, or only the long wave components of the flow, or only limited regions of the Northern Hemisphere?
- Could we find better analogs if we filtered the data to remove the highest temporal frequencies?

In this paper, we shall search time series of Northern Hemisphere wintertime geopotential heights for possible analogs. We shall repeat the search several times, filtering the data in various ways to reduce the number of degrees of freedom contained in the original data.

As an initial simplification, we shall restrict our attention to the 500 mb level. Thus, we disregard completely the vertical structure of the flow. We took this step for several reasons. First, we were quite convinced by Lorenz's results that we would not find close analogs if we considered the three-dimensional flow. Second, we felt that there was some physical justification for truncating the number of degrees of freedom of the flow in this way. By neglecting all levels but 500 mb, we effectively retain only a barotropic representation of the flow, since this level is close to the steering level in middle latitudes. However, barotropic models of the atmosphere, pioneered by Charney and Eliassen (1949), have demonstrated remarkable success in reproducing the mean state and time evolution of atmospheric motions. Of course, if we were to find an abundance of good analogs using only the 500 mb height field, we could then screen the analogs further by reintroducing other levels.

We conducted eighteen analog searches over our wintertime 500 mb height data, by defining analog pairs in three ways (or "types") based on six subsets of the daily time series. Analog definitions and data filtering techniques are described in Section 2 of this paper. Maps of the best analog pairs are presented in Section 3. We then examined the increase with time of the difference between the observed flows succeeding the analogs. This "error growth" was compared to the corresponding error growth associated with pure persistence. These results are discussed in Section 4. Some conclusions follow in Section 5.

2. Data and analysis procedure

Our data set consists of daily 0000 GMT Northern Hemisphere 500 mb height observations for a 15-year period (January 1963–December 1977). The data were derived from NMC operational analyses and obtained from the NCAR data archive. The data are represented on a 4° latitude by 5° longitude grid. Temporal linear interpolation was performed to replace a few missing or obviously erroneous grids. The annual and semiannual cycles were defined by calculating the 15th and 30th Fourier harmonics from the entire 15-year time series at each gridpoint. These fluctuations, incorporating the spectral components with periods of one year and six months, were removed from the data, defining 500 mb height anomalies.

For this study, we considered the set of 500 mb height anomaly maps for the months of December, January, and February only—a total of 1354 days. Maps were compared over the midlatitude region between 30 and 70°N. South of 30° and north of 70° we judged the NMC analyses to be less reliable than over middle latitudes. The 500 mb height variability is small southward of 30° relative to middle latitudes (Blackmon, 1976), so geopotential height is probably not the most meaningful parameter to define analogs there. We felt that restricting our attention to middle latitudes would both increase the reliability of our results and save considerable computing time.

Analogs were defined in three ways, each of which shall be referred to as an "analog type":

1) Total root mean square (RMS) difference. For each two maps A and B, where A_j and B_j are 500 mb height anomalies scaled by the cosine of latitude for gridpoints $j = 1, 2, \ldots, N$ (N the total number of gridpoints), the area-weighted root mean square difference between the maps is given by

$$\mathrm{RMS} = \left(\frac{1}{N}\sum_{j=1}^{N}(B_j - A_j)^2\right)^{1/2}. \tag{1}$$

The best analogs using this criterion are the pairs of maps (A, B) that minimize RMS.

2) Spatial covariance (COV). The spatial covariance between A and B is given by

$$\overline{AB} - \bar{A}\bar{B}, \tag{2}$$

where the overbar represents an average over the area-weighted grid points.

3) Spatial correlation (COR). The spatial correlation between A and B is given by

$$\mathrm{COR} = \frac{\mathrm{COV}}{\sigma_A \sigma_B}, \quad \text{where} \quad \sigma_A = (\overline{A^2} - \bar{A}^2)^{1/2}. \tag{3}$$

The best analogs defined using the COV and COR criteria are the pairs (A, B) which maximize those quantities.

Each analog type emphasizes somewhat different aspects of the circulation patterns. The RMS type is most sensitive to the amplitude of the anomaly pattern, and less sensitive to accurate matching of the phase of the pattern at all locations. High covariance will occur if the more pronounced highs and lows on a map are matched, with less emphasis on areas where the anomaly is small. Even perfectly matched patterns

could have a low covariance if they contained no large-amplitude anomalies. The correlation type is most sensitive to the phase of the pattern, with less preference given to large-amplitude anomaly patterns.

Analog types were defined after removing degrees of freedom from the data set in six different ways, each of which shall be referred to as a "subset":

1) *Total field.* These were the 500 mb height anomalies as previously described.

2) *Long waves only.* Fourier decomposition was performed around each latitude circle. For this subset, only zonal wavenumbers 0 through 4 were retained.

3) *Short waves only.* This subset contained the remainder of the variability of each pattern after the long waves were removed for subset 2). Since our grid resolution was 5° in the longitudinal direction, this subset contains fluctuations with zonal wavenumbers 5 through 36.

4) *Five-day mean anomalies.* The daily time series were grouped into running 5-day means before the analog search was conducted. The area considered was identical to subsets 1), 2), and 3).

5) *European sector only.* For this subset we considered only the 500 mb anomaly field east of 15°W and west of 60°E (with the same southern and northern bounds as before). The total anomaly field within this region was used.

6) *North American sector only.* The total anomaly east of 180°W and west of 60°W was considered for this subset.

Analog searches were conducted for each combination of analog type and data subset.

For each data subset and analog type, every map within a single winter was compared with all maps from other winters only. This procedure was followed to ensure that a good analog pair was not merely due to persistence, but actually represented recurrence of a circulation pattern. The total number of analog pairs contained in our data set using this procedure was 857 375.

3. Analog quality

Table 1 contains lists of the ten best independent analog pairs for each of the six data subsets and three analog types described in Section 2 and the mean rms difference over all pairs. The independence of the analog pairs was subjectively determined by examining the lists of the best analogs for each subset and analog type. The selection process is illustrated in Table 2, which contains the 20 best analog pairs based on COR values for long waves only. Because 500 mb height anomalies are quite persistent from day to day (Gutzler and Mo, 1983), many of the best analog pairs are representative of the same synoptic situation with one map differing by a day or two from another analog pair. For calculations of error growth rates (Section 4), we desired to average the ten best independent pairs. Hence, the second, fourth, fifth, seventh, ninth, 14th, 15th, and 17th best pairs in Table 2 were not included in Table 1 because they were representative of the same synoptic situation as the best pair. In addition, we dropped analog pairs in which one or both dates occurred within ten days of the end of February (such as the tenth and eleventh best analog pairs in Table 2), so that we could calculate ten days of error growth.

We begin our discussion of Table 1 by examining the entries for the total anomaly field. The analog selection process using this subset is most similar to that of Lorenz (1969b), and therefore it is not surprising that these results are also similar. The best total-field analogs based on COR explain just over half the total variance between maps. The rms difference between even the best analog pairs in this subset (90.1 m) is slightly greater than half the difference between randomly chosen maps. This rms difference represents an improvement of about 15% over the best analog pairs found by Lorenz. By comparison, Leith (1978) has estimated that the hemispheric rms error in the 500 mb height field associated with observational uncertainty and interpolation to gridpoint values is about 15 meters.

The quality of the best analogs found in the data set can be judged visually by the plots shown in Fig. 1, in which the maps of one of the best analog pairs, 721204 and 740106, are presented. This was the best analog pair based on COV values for the total field, and third best among analogs based on COR. Figs. 1(a) and 1(b) contain the anomaly maps upon which the analog statistics were based; Fig. 1(c) shows the difference between the anomalies; and Figs. 1(d) and 1(e) contain the complete 500 mb height fields for the two dates with the seasonal cycle retained. Keep in mind that only the region between latitude circles 30 and 70°N (which are marked by heavy lines) was considered for the calculation.

Each map contains a highly positive anomaly centered over the Gulf of Alaska, a negative anomaly which is strongest over the North Atlantic and extends westward across North America, and anomalies alternating in sign in a similar fashion across northern Asia. The difference map, however, reveals that relatively small dissimilarities in the positions and magnitudes of the anomalies on the two maps translate into large local differences between the maps. The North Atlantic anomaly on 740106 extends farther southward than the corresponding anomaly on 721204, resulting in a large negative difference east of Labrador in Fig. 1(c). The positive anomaly over northern Europe on 740106 is located to the northwest of its position on 721204, so that the difference between maps is greater than 400 m near Scandinavia. Comparison of the complete 500 mb height fields for the two dates yields qualitatively similar results: some general agreement between

TABLE 1. Lists of the ten best independent analog pairs for each data subset and analog type. See text for details concerning the subsets and types. The first two digits in each date represent the year; the second two digits represent the month; the last two digits represent the day; 0000 GMT data is used for all cases (e.g., 641204 means 0000 GMT 4 December 1964). Also listed for each data subset are the average RMS value of all possible analog pairs, and the estimated doubling time of RMS errors averaged over the ten best RMS analog pairs.

		RMS (%)	COV		COR	
			Total anomaly field			
1	641204–741212	90.1 51	721204–740106	16 867	740110–771209	0.735
2	650113–750119	96.8 55	661205–680130	16 751	661205–680130	0.731
3	680108–670105	97.8 56	630131–641222	15 893	721204–740106	0.725
4	740217–761220	99.2 57	740110–771209	15 358	721212–750129	0.692
5	721224–771215	99.3 57	630130–680217	15 204	680118–740118	0.690
6	661221–741212	99.6 57	710112–740106	15 139	730109–750206	0.690
7	750104–760112	100.2 57	630114–671229	15 100	650113–650119	0.687
8	640103–760217	100.4 57	640120–671203	15 046	740103–760205	0.680
9	640102–721226	101.0 58	690214–691205	15 002	691206–741211	0.679
10	691225–741213	103.3 59	651227–661201	14 927	730123–771215	0.679
	$\overline{RMS}$ = 175.0 m Doubling time = 7.4 days					
			Waves 0–4 only			
1	691225–741213	61.1 40	721204–740106	16 893	740109–771209	0.824
2	631208–760202	66.3 44	630131–641222	15 450	650112–750119	0.820
3	650112–750119	67.4 45	740109–771209	15 035	721204–740106	0.814
4	680108–760105	68.7 46	661205–680130	14 388	721212–750129	0.807
5	691224–711202	71.5 47	710112–740106	14 379	661205–680130	0.795
6	631228–701213	71.9 48	681230–761230	14 301	661227–770101	0.781
7	641210–741221	72.3 48	630130–680217	14 231	730109–750206	0.780
8	711210–751211	72.5 48	640120–671203	14 111	690102–710203	0.777
9	731210–751223	72.6 48	690217–761230	14 077	760125–770110	0.777
10	731211–750104	72.7 48	661224–761230	13 638	680108–760105	0.769
	$\overline{RMS}$ = 150.9 m Doubling time = 6.5 days					
			Waves 5–36 only			
1	721224–760218	41.9 51	631201–721217	6641	631201–750114	0.779
2	760217–770114	42.2 51	631201–760203	6209	720205–721217	0.770
3	740130–751228	42.3 51	631201–710210	5938	631201–720205	0.763
4	760116–761207	42.4 51	631201–750114	5911	631225–731222	0.760
5	631213–770114	42.8 52	631226–731223	5761	651208–690114	0.758
6	760217–770213	43.3 53	671219–701217	5526	630121–710209	0.758
7	720214–741218	43.3 53	631201–720205	5479	631201–721217	0.757
8	730121–741211	43.4 53	680129–711224	5462	680211–720205	0.756
9	630218–721220	43.5 53	661203–690105	5451	631201–680209	0.755
10	750123–770211	43.5 53	710129–731223	5447	630112–711215	0.755
	$\overline{RMS}$ = 82.4 m Doubling time = 6.3 days					
			Five-day mean anomalies			
1	670112–760113	68.6 48	721203–740103	14 270	740112–771209	0.781
2	651216–741219	71.2 50	740109–771207	12 761	661221–691204	0.775
3	631230–721225	72.1 50	690212–691203	11 988	721202–740103	0.767
4	641203–741212	72.5 50	641227–651226	11 807	661224–761230	0.756
5	750102–760110	73.2 51	710109–740104	11 637	721209–750126	0.741
6	721226–760214	74.6 52	710110–750131	11 430	641228–651227	0.739
7	731220–770212	75.2 52	661203–680128	11 412	650111–750118	0.739
8	661219–741210	75.6 53	690101–710129	11 189	730107–750204	0.724
9	720209–740212	76.3 53	651225–661201	11 170	681201–720104	0.724
10	641201–760122	76.4 53	630129–641219	11 145	680116–740116	0.723
	$\overline{RMS}$ = 143.7 m Doubling time = 11.3 days					

TABLE 1. (*Continued*)

		RMS (%)	COV		COR	
			European sector only			
1	721205–750118	53.0 31	640116–750208	27 997	671207–760124	0.936
2	730112–770115	54.1 32	630205–730215	25 884	640116–750208	0.930
3	720210–740204	56.7 33	730214–761206	25 738	710113–720102	0.922
4	750201–771213	57.6 34	630205–761205	25 424	651204–740207	0.919
5	670127–770209	59.3 35	640120–721219	24 842	670113–751226	0.908
6	740204–770125	59.9 35	710114–720103	24 576	681205–710114	0.907
7	650101–750124	60.0 35	630205–690215	23 760	700104–761229	0.906
8	710122–740214	60.2 36	640118–701211	23 737	681202–730111	0.903
9	680212–690112	60.3 36	710207–730109	23 363	721205–750118	0.903
10	721203–740216	60.7 36	730110–750207	23 233	650118–761201	0.901
	$\overline{\text{RMS}}$ = 169.4 m Doubling time = 3.9 days					
			North American sector only			
1	750104–760219	63.2 34	630209–680212	34 465	721208–740105	0.909
2	701212–741212	68.6 37	721208–740103	33 064	641219–710112	0.900
3	670208–750119	71.4 39	680211–761230	32 038	650117–680208	0.895
4	720117–751204	72.5 39	651229–711222	30 201	661205–680130	0.893
5	670103–681203	73.2 40	630131–641222	30 029	630115–671228	0.891
6	741214–751228	73.7 40	680212–770117	29 895	641228–651231	0.891
7	671209–741220	73.9 40	651229–701201	29 416	661206–701201	0.889
8	640105–741226	74.0 40	661205–680130	29 352	670208–750119	0.877
9	640201–751227	74.1 40	661205–701201	29 185	651229–711222	0.875
10	650110–761211	74.3 40	680129–701201	29 044	650117–700209	0.868
	$\overline{\text{RMS}}$ = 183.8 m Doubling time = 4.9 days					

TABLE 2. The list of the twenty best correlation analog pairs for the long waves only data subset. An asterisk is shown to the right of each pair appearing in the corresponding list in Table 1. A number *n* is shown to the right of each pair not considered further because it was judged to be not independent of the *n*th best analog pair. An *F* is shown to the right of each pair not considered further because it appeared too late in February to allow a growth rate calculation.

	Waves 0–4	COR	
1	740109–771209	0.824	*
2	740110–771209	0.823	1
3	650112–750119	0.820	*
4	740113–771209	0.819	1
5	740113–771210	0.817	1
6	721204–740106	0.814	*
7	740110–771210	0.811	1
8	721212–750129	0.807	*
9	740109–771210	0.805	1
10	710112–720225	0.803	*F*
11	671202–740226	0.802	*F*
12	721204–740107	0.802	6
13	661205–680130	0.795	*
14	740112–771209	0.791	1
15	740114–771210	0.791	1
16	650113–750119	0.789	3
17	740112–771210	0.789	1
18	721213–750130	0.787	8
19	721212–750130	0.784	8
20	721204–740103	0.781	6

the maps with regard to broad scale features, but sufficient dissimilarity to create large local differences.

Comparing the lists of dates for the total field analogs, we see that many of the same analog pairs appear for each of the three analog types. Many more redundant analog pairs were removed from the lists for subset COV than from lists for the other types, indicative of the sensitivity of that statistic to the presence of one or two very large anomalies (which often persist for several days).

We also observe that lists of the best analogs for subsets based on the total field and the long waves only have many pairs in common. This is consistent with the observation that most of the variance of the 500 mb height field is contained in the long waves (Blackmon, 1976). We observe further that the magnitudes of the best covariances in these subsets are about the same, whereas the best RMS values are lower, and the best COR values are higher (both indicating improved analog quality), when the long waves only are considered. The best analog pair as measured by rms for the long-wave subset contains only 40% of the error between randomly chosen maps. Hence, we deduce that most of the similarity between maps comprising the best analog pairs for the total-field subset is in fact due to matching of the long-wave patterns,

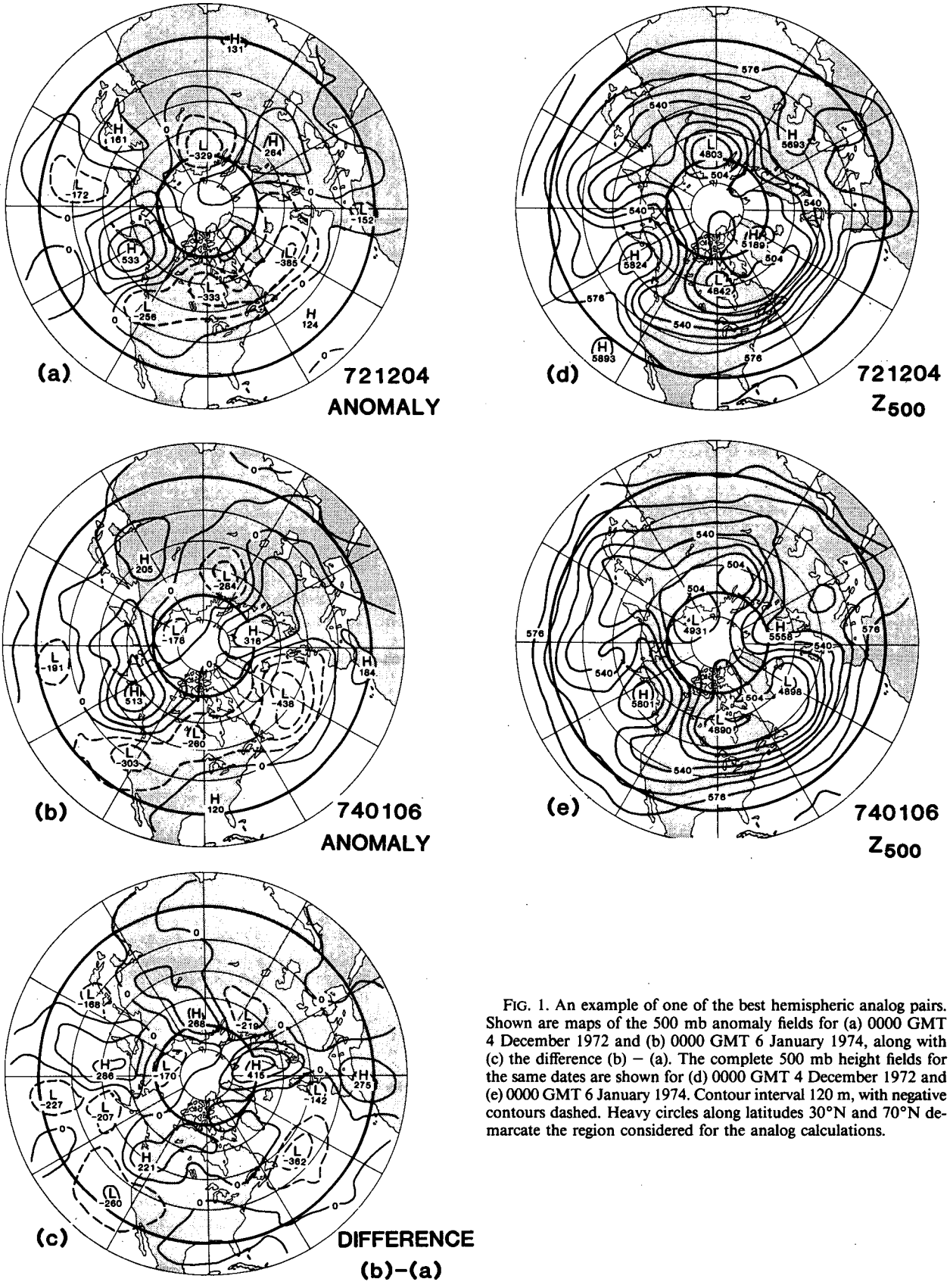

FIG. 1. An example of one of the best hemispheric analog pairs. Shown are maps of the 500 mb anomaly fields for (a) 0000 GMT 4 December 1972 and (b) 0000 GMT 6 January 1974, along with (c) the difference (b) − (a). The complete 500 mb height fields for the same dates are shown for (d) 0000 GMT 4 December 1972 and (e) 0000 GMT 6 January 1974. Contour interval 120 m, with negative contours dashed. Heavy circles along latitudes 30°N and 70°N demarcate the region considered for the analog calculations.

with the short waves contributing little to (or, as in the case of the best long wave COV pair, degrading) the similarity.

These conclusions are supported by visual inspection of the plotted maps for the best analog pairs. Long wave maps for dates 721204 and 740106 are presented in Fig. 2 for comparison with the maps of the unfiltered anomaly field previously shown in Fig. 1.

The low covariances observed in Table 1 for the short wave subset also are consistent with the notion that most of the variance is contained in the long waves. Because of this, RMS values are low for the short wave analogs; however, the ratio of analog error to random error is again over one-half, even for the best pairs. The short wave analog lists based on COV and COR are dominated by a few interrelated maps which do contain substantial anomalies.

Filtering the data temporally by computing five-day running means also improves analog quality, but not as effectively as removing the short waves. We see from Table 1 that analog quality is somewhat poorer in this subset compared to the long-wave subset, despite the removal of slightly more of the total variance, as indicated by the lower value of RMS. Several analog pairs are common to the total field, long wave, and five-day mean subsets. In Fig. 3 are presented the mean 500 mb height fields (with the seasonal cycle included) for the five-day periods centered on 721204 and 740105.

By restricting attention to only a sector of the hemisphere, we substantially reduce the number of spatial degrees of freedom contained in each map, so it is not surprising that COV and COR values for the best analogs are quite high—correlations are around 0.9. The

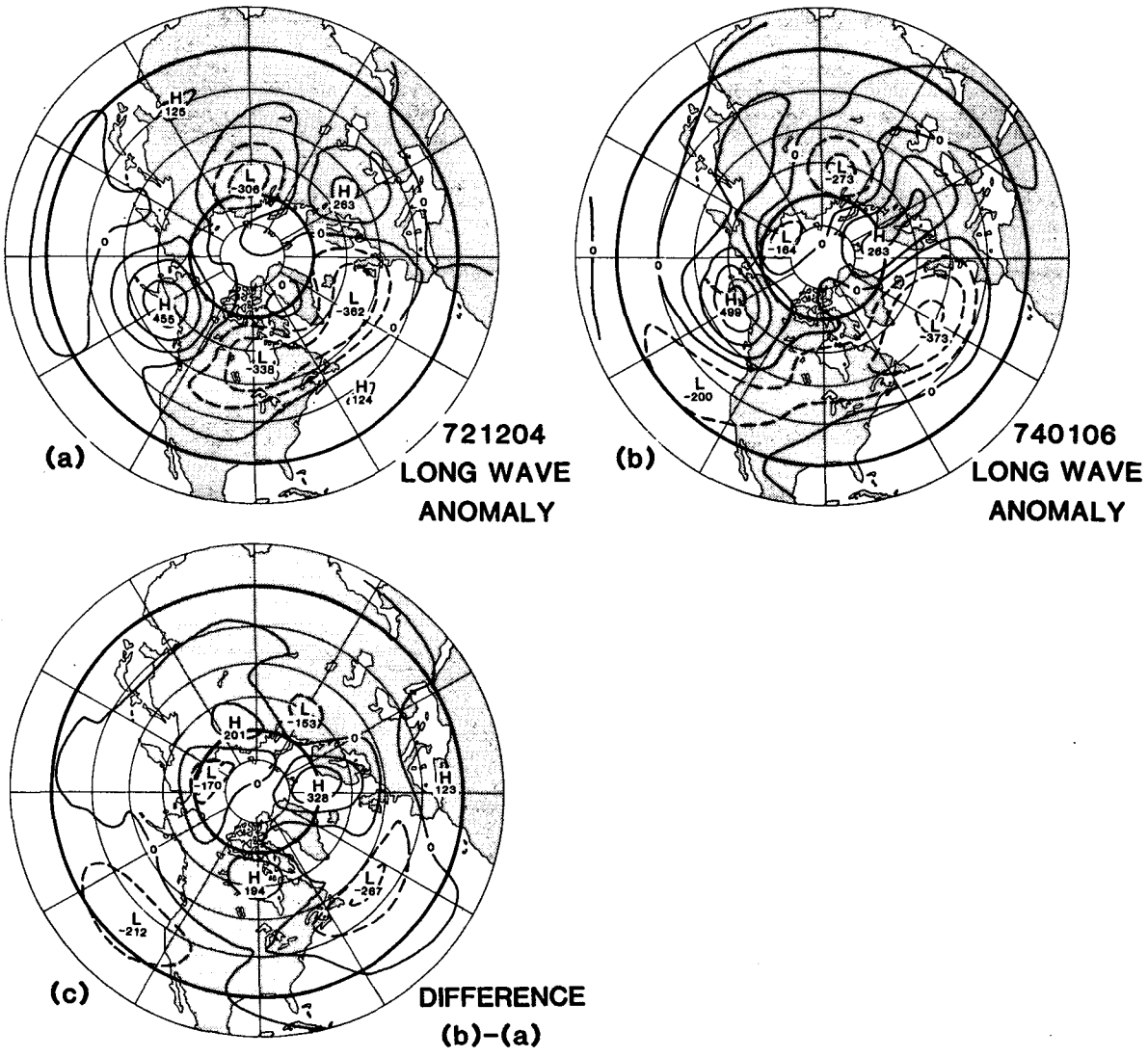

FIG. 2. As in Fig. 1(a)–(c) but with zonal wavenumbers higher than 4 subtracted from the data.

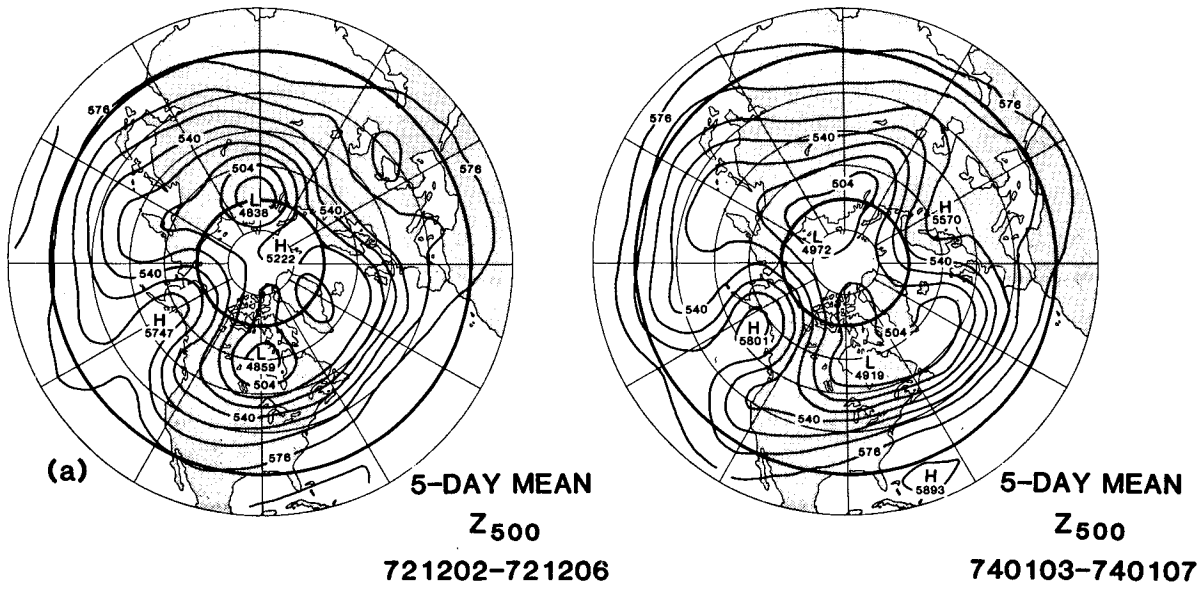

FIG. 3. Five day mean 500 mb height map centered on (a) 5 December 1972 and (b) 5 January 1974.

rms differences between the best analogs are only about one-third the difference between randomly chosen maps, however, suggesting that the improvement in analog quality is somewhat greater than one would expect if we had selected the sector boundaries randomly. In fact, the European and North American sectors were defined so that they would correspond to the locations of prominent teleconnection patterns (denoted EA and PNA, respectively) in the monthly mean 500 mb height field (Wallace and Gutzler, 1981). We were interested in investigating the possibility that these teleconnection patterns might act as "waveguides" to channel transient fluctuations, thus increasing the chances of finding good analogs whose difference would grow slowly with time, since the background teleconnection would presumably persist as a quasi-stationary feature of the long waves.

Maps for one of the best analog pairs within the North American subset, 670208 and 750119, are shown in Fig. 4. This analog pair was among the ten best using RMS and COR criteria. Within the computational domain considered for the analog comparison, the 500 mb height patterns are quite similar. However, large differences between the patterns exist just outside the computational domain on the difference plot (Fig. 4c). One might suspect that such differences might rapidly degrade the analog quality of the pairs of maps succeeding 670208 and 750119. This was indeed the case; in the next section we shall discuss the error growth of analog quality with time in more detail.

4. Error growth rates

In Section 3 it was demonstrated that the degree of similarity between the best analogs (as measured by the spatial correlation, covariance, or rms difference) could be improved by eliminating degrees of freedom from the 500 mb height time series by spatial or temporal filtering or by considering only a sector of the hemisphere. In this section we will examine the utility of the analogs for forecasting purposes by comparing the decline of the similarity of the analog pairs defined by the dates immediately succeeding the best analog pair with the error growth of a persistence forecast.

Analogs defined using only a subset of the complete flow are not necessarily useful for forecasting the evolution of the flow, even if the analogs are very similar. For instance, we could continue to remove degrees of freedom from the data until we define a purely local analog: the 500 mb height at a single gridpoint. We could surely find many high quality analogs using this definition (or even "perfect" quality analogs in the event of equal height anomalies). However, such analogs would probably not be very useful for forecasting purposes, because they would contain little information concerning the nature of the large-scale flow in which they were imbedded.

We measured the forecast utility of the analog pairs listed in Table 1 in the following way. We calculated a linear average of the similarity—rms error, covariance, or correlation—of the ten analog pairs for each subset. This average was then recalculated after stepping ahead one day from each date, and so on for ten days. This allowed us to chart the decay of the analog similarity for a ten-day period.

The decay of analog similarity corresponds to the error growth of a forecast. In this spirit, we can imagine that maps succeeding the earlier date of each analog pair were used as predictors of the maps succeeding the later date. We can then compare the error growth

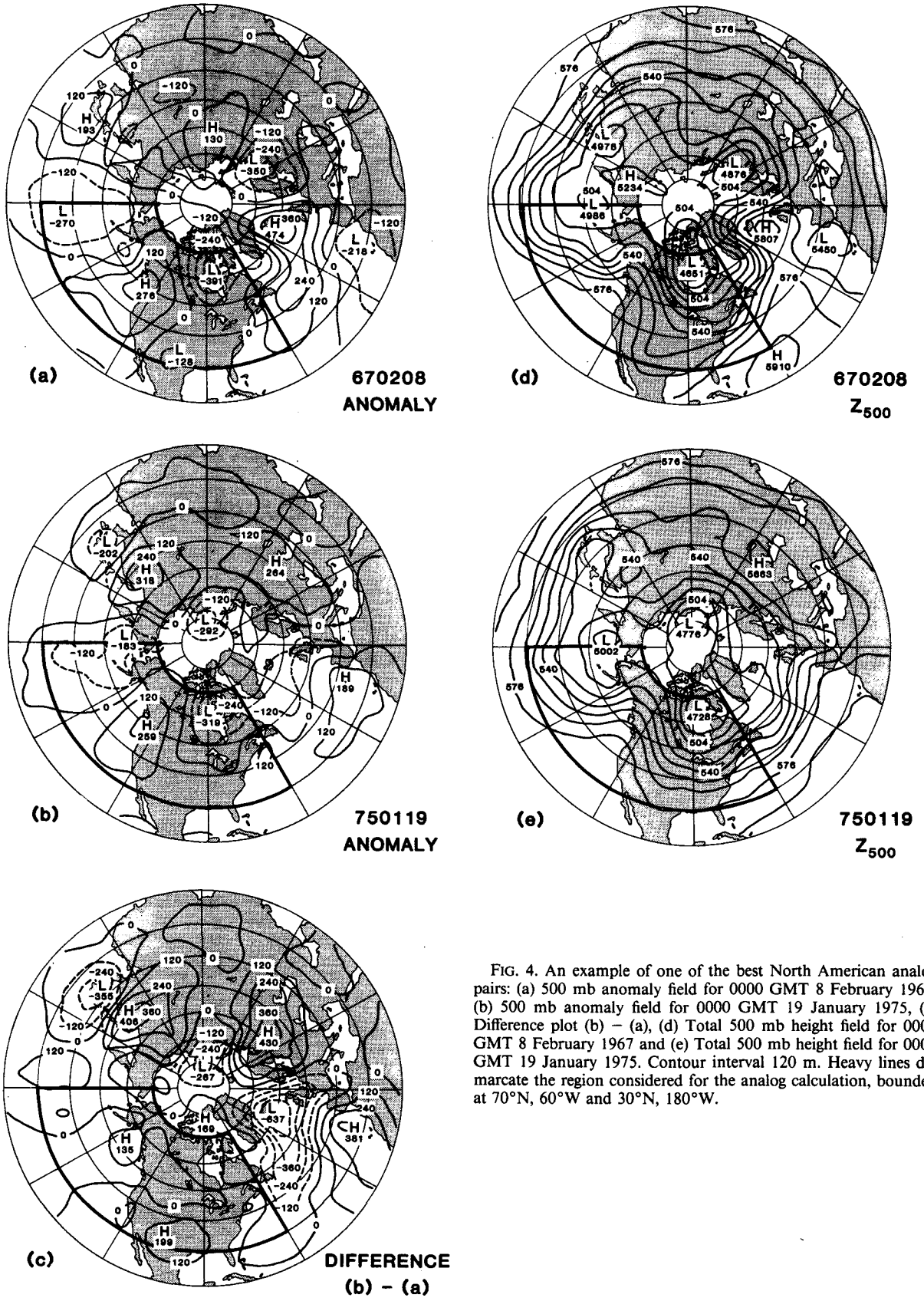

FIG. 4. An example of one of the best North American analog pairs: (a) 500 mb anomaly field for 0000 GMT 8 February 1967, (b) 500 mb anomaly field for 0000 GMT 19 January 1975, (c) Difference plot (b) − (a), (d) Total 500 mb height field for 0000 GMT 8 February 1967 and (e) Total 500 mb height field for 0000 GMT 19 January 1975. Contour interval 120 m. Heavy lines demarcate the region considered for the analog calculation, bounded at 70°N, 60°W and 30°N, 180°W.

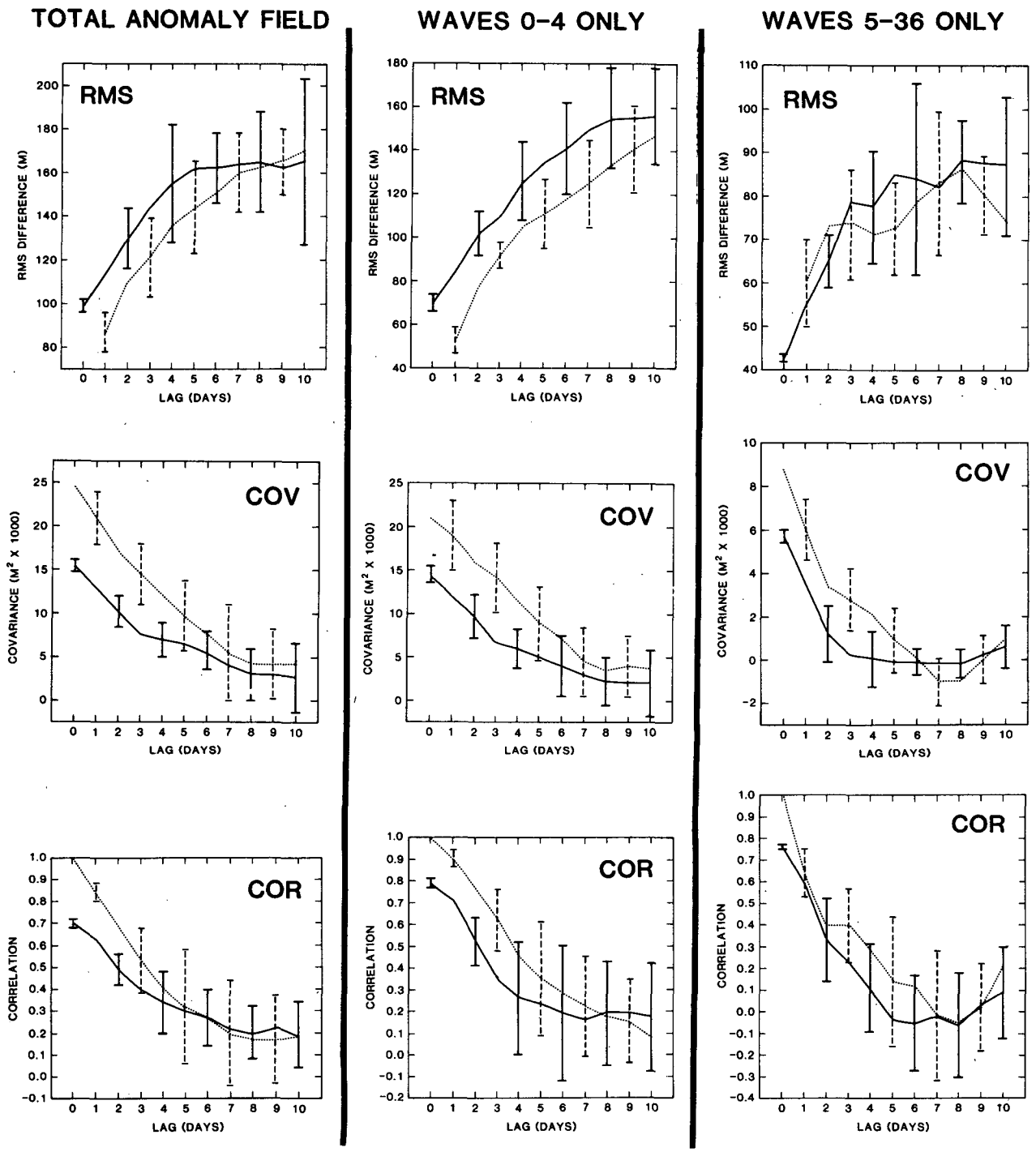

FIG. 5. Error growth curves for each subset and analog type considered. The solid curve in each plot represents an average over the ensemble of the ten best analogs, with the uncertainty of the average (plus and minus one standard deviation of the ensemble) shown as solid bars. The dashed curve and bars represent the corresponding average of persistence forecasts for the same set of dates.

of the analog forecast with the error growth of a persistence forecast for the same set of ten dates.

Error growth plots for each analog subset are shown in Fig. 5. The solid curve in each plot represents the average similarity of the analog forecast, with the uncertainty of the calculations (defined as plus or minus one standard deviation of the ensemble of ten individual forecasts) shown as solid error bars. The dashed curve and error bars in each plot represent the quality of a persistence forecast in the same way.

In every case, the persistence forecast does no worse, and often is significantly better, than the analog fore-

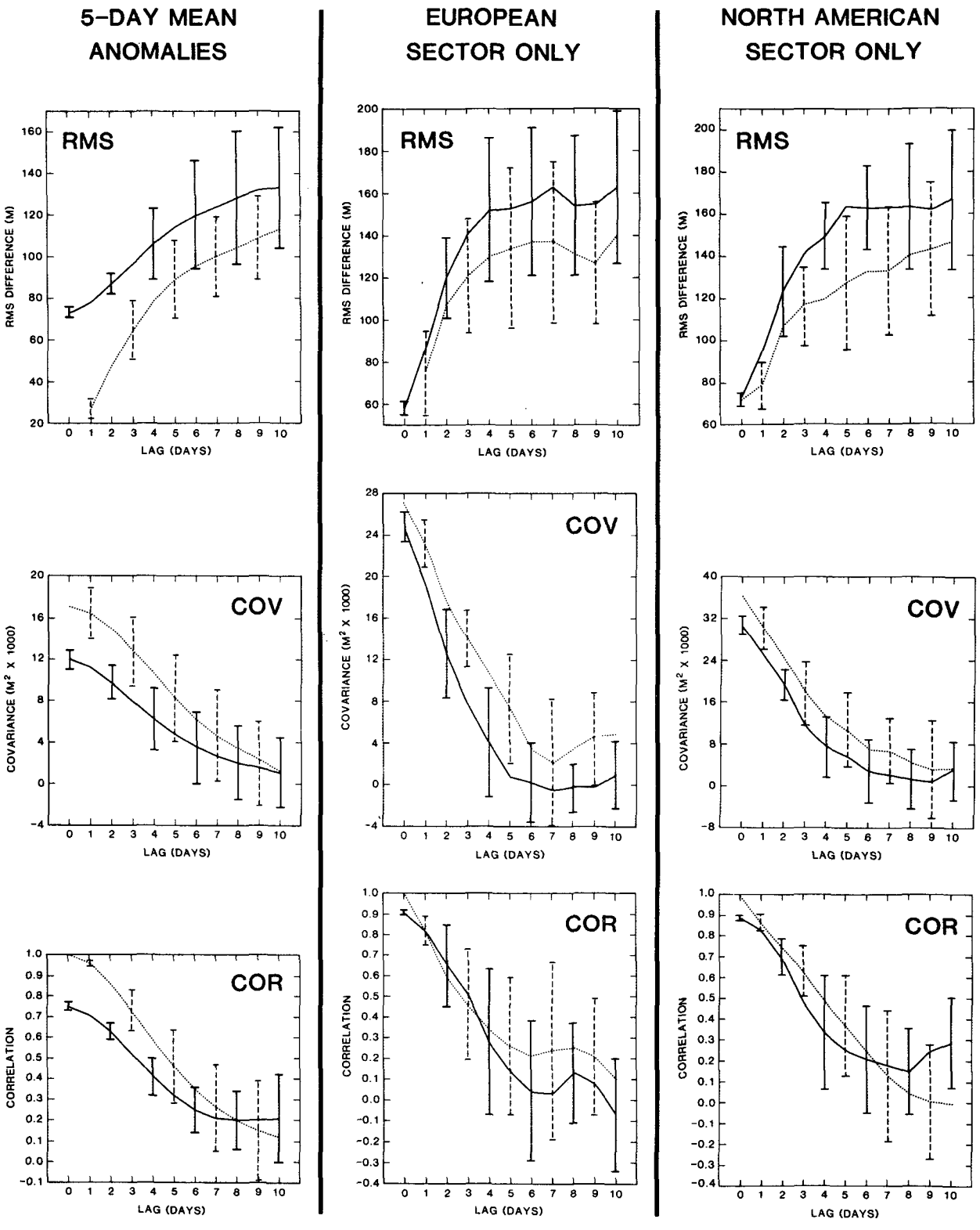

FIG. 5. (*Continued*)

cast. Apparently, the analogs listed in Table 1 have very little forecast utility.

An alternative assessment of error growth can be made by estimating the doubling time for errors associated with the best RMS analog pairs for each data subset. Following the method outlined by Lorenz

(1969b), the average doubling time T for each subset is defined as

$$(1 + \Delta)^T = 2 \quad \text{where} \quad \Delta = \frac{\text{RMS}_2 - \text{RMS}_1}{\overline{\text{RMS}}}. \quad (4)$$

Here RMS_2 and RMS_1 are the RMS errors between the maps succeeding the dates listed in Table 1 by two days and one day, respectively. RMS_2 and RMS_1 were averaged over the ten cases for each subset. The doubling times are included in Table 1.

Lorenz estimated a doubling time of 8 days from (4) for errors corresponding to the best analogs in his data sample. That number is close to the doubling time that we calculate for our total anomaly field analogs, 7.4 days. This is considerably longer than the estimated doubling time of about 2½ days derived from dynamical studies associated with very small perturbations (Lorenz, 1969a). The doubling times are somewhat reduced from the total anomaly case for the subsets which incorporate only long waves (6.5 days) or short waves (6.3 days). This suggests that the short waves which had been filtered out of the long wave subset act to degrade the succeeding long-wave analog pairs. The long doubling time associated with the five-day mean analogs can probably be attributed to the averaging process, since running five-day means separated by one day contain four days' data in common. The doubling times for the sector analogs are extremely short, about four days for each subset, indicative of very rapid degradation. In each case, the doubling time estimates are consistent with visual examination of the RMS error growth plots shown in Fig. 5.

5. Discussion

We have attempted to improve the quality of analogs found in a 15-winter sample of Northern Hemisphere 500 mb height grids by removing degrees of freedom from the flow by spatial filtering or temporal averaging. We started our investigation by simplifying the flow patterns relative to those considered by Lorenz (1969b), with the hope that we could thereby decrease the difference between the best analogs. Although some improvement was achieved, the resulting analogs were no more useful for forecasting subsequent 500 mb height maps than simply assuming that the original flow would persist. The error growth of an analog forecast was found to be comparable to the error growth of a persistence forecast; therefore, since each persistence forecast was initially error-free, the analog forecast was consistently poorer.

Our results imply that these analogs are not a useful tool for forecasting the evolution of the midlatitude flow on time scales of several days. Neglect of the polar region, the subtropics, and all levels except 500 mb resulted in somewhat better analogs and therefore smaller initial errors within the computational domain; however, the errors outside the computational domain quickly propagated to the midlatitude 500 mb height field and contaminated the analog forecasts.

The importance of horizontal advection of errors was investigated for the set of North American analogs listed in Table 1. Error growth calculations similar to those displayed in Fig. 5 were made for several smaller computational domains within the boundaries used to calculate the analogs. The results (not shown) were quite similar to those presented in Fig. 5: rapid error growth and no improvement over persistence realized by the analog forecast. Apparently, horizontal advection is not the primary cause of contamination. Horizontal propagation of wave energy can take place more quickly than an advective time scale would imply, however. Somerville (1980) presented evidence of extremely rapid contamination of numerical weather forecasts for Northern Hemisphere middle latitudes by errors in the initialization field in the tropics.

Vertical propagation of errors could be a major source of contamination in the analog forecasts as well. An interesting extension of the current work would be to investigate the relative importance of vertical and horizontal energy propagation in the forecast contamination.

Comparison of analog forecast degradation with persistence could be somewhat misleading if the best analogs were more persistent than randomly selected maps. An indication that this might be so comes from comparing the lists of dates in Table 1 with the lists of dates of large persistent anomalies ("blocking" events) presented by Charney *et al.* (1981). Using the same data set employed here (excluding December 1977), they identified 36 separate events in which a 500 mb height anomaly at a single gridpoint along 50, 60 or 70°N, of magnitude 200 m or greater, persisted for at least seven days (their Tables 2 and 3, plus two events mentioned in the text above Table 3). These events spanned a total of 392 days out of 1319 days in their data set (30%). Of the eighteen dates listed in Table 1 for total-field rms analogs, five occur within a blocking event, while thirteen of eighteen total field covariance analogs include blocks. Hence, high covariance tends to be associated with blocking.

Our negative results should not be extended to other applications of analog forecasting. The point-by-point comparison of geopotential height anomalies used here to compare two atmospheric states is not necessarily the most appropriate technique for judging their similarity. Two height fields which are identical except for a 20° shift in phase would not be considered as a good analog pair in our computations, although their subsequent dynamical evolution might be fairly similar. One could envision that a clever scheme that quantifies concepts such as the strength of the jet streams might produce higher quality, more useful analogs.

It is also possible that we have not chosen the best method for reducing the degrees of freedom of a point-

by-point calculation. Perhaps consideration of the largest spatial scales of global data—the lowest order spherical harmonics or Hough modes, for example—would yield better results.

Acknowledgments. We are deeply indebted to Mr. Brian Doty for his contributions to the computational process and the interpretation of the results. We appreciate the help we received from Ms. Laura Rumburg, who drafted the figures, and Ms. Jody Reckley and Ms. Debbie Sabatino, who typed the manuscript.

REFERENCES

Barnett, T. P., and R. W. Preisendorfer, 1978: Multifield analog prediction of short-term climate fluctuations using a climate state vector. *J. Atmos. Sci.*, **35**, 1771–1787.

Baur, F., 1948: *Einfuhrung in die Grosswetterkunde.* Wiesbaden, Dieterich, 165 pp.

Blackmon, M. L., 1976: A climatological spectral study of the 500 mb geopotential height of the Northern Hemisphere. *J. Atmos. Sci.*, **33**, 1607–1623.

Charney, J. G., and A. Eliassen, 1949: A numerical method for predicting the perturbations of the middle latitude westerlies. *Tellus*, **1**, 38–54.

——, J. Shukla and K. C. Mo, 1981: Comparison of a barotropic blocking theory with observation. *J. Atmos. Sci.*, **38**, 762–779.

Gutzler, D. S., and K. Mo, 1983: Autocorrelation of Northern Hemisphere geopotential heights. *Mon. Wea. Rev.*, **111**, 155–164.

Horel, J., 1981: A rotated principal component analysis of the interannual variability of the Northern Hemisphere 500 mb height field. *Mon. Wea. Rev.*, **109**, 2080–2092.

Leith, C. E., 1973: The standard error of time-average estimates of climatic means. *J. Appl. Meteor.*, **12**, 1066–1069.

——, 1978: Objective methods for weather prediction. *Annual Review of Fluid Mechanics*, Vol. 10, Academic Press. 107–128.

Lorenz, E. N., 1969a: Three approaches to atmospheric predictability. *Bull. Amer. Meteor. Soc.*, **50**, 345–349.

——, 1969b: Atmospheric predictability as revealed by naturally occurring analogs. *J. Atmos. Sci.*, **26**, 636–646.

Martin, D. E., 1953: Anomalies in the Northern Hemisphere 5-day mean circulation patterns. Air Weather Service Rep. No. 105-100, 39 pp.

O'Connor, J. T., 1969: Hemispheric teleconnections of mean circulation anomalies at 700 mb. ESSA Tech. Rep. WB-10, 103 pp.

Schuurmans, C., 1973: A 4-year experiment in long-range weather forecasting, using circulation analogs. *Meteor. Rundsch.*, **26**, 2–4.

Somerville, R. J. E., 1980: Tropical influences on the predictability of ultralong waves. *J. Atmos. Sci.*, **37**, 1141–1156.

Walker, G. T., and E. W. Bliss, 1932: World Weather V. *Mem. Roy. Meteor. Soc.*, **4**, 53–84.

Wallace, J. M., and D. S. Gutzler, 1981: Teleconnections in the geopotential height field during the Northern Hemisphere winter. *Mon. Wea. Rev.*, **109**, 784–812.